REPORT DOCUMENTATION PAGE

Form Approved OMB NO. 0704-0188

1. REPORT DATE (DD-MM-YYYY)	2. REPORT TYPE	3. DATES COVERED (From - To)
06-11-2012	Final Report	20-Jun-2009 - 19-Jun-2012

4. TITLE AND SUBTITLE
Final Progress Report for Grant Number W911NF-09-1-0347

5a. CONTRACT NUMBER
W911NF-09-1-0347

5b. GRANT NUMBER

5c. PROGRAM ELEMENT NUMBER
611102

6. AUTHORS
Matthew J. Gilbert

5d. PROJECT NUMBER

5e. TASK NUMBER

5f. WORK UNIT NUMBER

7. PERFORMING ORGANIZATION NAMES AND ADDRESSES
University of Illinois - Urbana
OSPRA
The Board of Trustees of the University of Illinois
Champaign, IL 61820 -7406

8. PERFORMING ORGANIZATION REPORT NUMBER

9. SPONSORING/MONITORING AGENCY NAME(S) AND ADDRESS(ES)
U.S. Army Research Office
P.O. Box 12211
Research Triangle Park, NC 27709-2211

10. SPONSOR/MONITOR'S ACRONYM(S)
ARO

11. SPONSOR/MONITOR'S REPORT NUMBER(S)
56054-PH.15

12. DISTRIBUTION AVAILIBILITY STATEMENT
Approved for Public Release; Distribution Unlimited

13. SUPPLEMENTARY NOTES
The views, opinions and/or findings contained in this report are those of the author(s) and should not contrued as an official Department of the Army position, policy or decision, unless so designated by other documentation.

14. ABSTRACT
The aim of this project is to explore the strongly correlated states, more specifically Bose-Einstein condensation of indirectly bound excitons, in bilayer graphene. During this final reporting period, we have continued our work on the extention of the many-body calculations to an atomistic model, examined the electron-phonon coupling, studied the possibility of finding the same type of condensation in a 3D topological insulator, and started our work on a time-dependent theory to understand the behavior of the time-dependent many-body systems. In this final progress

15. SUBJECT TERMS
graphene, many body, quantum monte carlo, superfluids, correlation

16. SECURITY CLASSIFICATION OF:			17. LIMITATION OF ABSTRACT	15. NUMBER OF PAGES	19a. NAME OF RESPONSIBLE PERSON
a. REPORT	b. ABSTRACT	c. THIS PAGE			Matthew Gilbert
UU	UU	UU	UU		19b. TELEPHONE NUMBER 217-333-3064

Report Title

Final Progress Report for Grant Number W911NF-09-1-0347

ABSTRACT

The aim of this project is to explore the strongly correlated states, more specifically Bose-Einstein condensation of indirectly bound excitons, in bilayer graphene. During this final reporting period, we have continued our work on the extention of the many-body calculations to an atomistic model, examined the electron-phonon coupling, studied the possibility of finding the same type of condensation in a 3D topological insulator, and started our work on a time-dependent theory to understand the behavior of the time-dependent many-body systems. In this final progress report, we will outline our most important results and draw some final conclusions from our 3 year project.

Enter List of papers submitted or published that acknowledge ARO support from the start of the project to the date of this printing. List the papers, including journal references, in the following categories:

(a) Papers published in peer-reviewed journals (N/A for none)

Received	Paper

TOTAL:

Number of Papers published in peer-reviewed journals:

(b) Papers published in non-peer-reviewed journals (N/A for none)

Received	Paper

TOTAL:

Number of Papers published in non peer-reviewed journals:

(c) Presentations

I gave invited presentations at the following conferences:

CIMTEC
"On the Possibility of Ultra-Low Power Switching in Multilayer Graphene Nanoribbons"

Nanotech
"On the Possibility of Ultra-Low Power Switching in Multilayer Graphene Nanoribbons"

Number of Presentations: 2.00

Non Peer-Reviewed Conference Proceeding publications (other than abstracts):

Received	Paper

TOTAL:

Number of Non Peer-Reviewed Conference Proceeding publications (other than abstracts):

Peer-Reviewed Conference Proceeding publications (other than abstracts):

Received	Paper

TOTAL:

Number of Peer-Reviewed Conference Proceeding publications (other than abstracts):

(d) Manuscripts

Received	Paper	
05/18/2010	1.00	M. Gilbert. Finite Temperature Pseudospin Torque Effect in Graphene Bilayers, (03 2010)
05/18/2010	2.00	J. Shumway, M. Gilbert. Path Integral Simulations of Quantized Conductance in Nanowires, (04 2010)
05/18/2010	3.00	M. Gilbert, J. Shumway. Probing quantum coherent states in bilayer graphene, (06 2009)
05/18/2010	4.00	J. Shumway, M. Gilbert. Formation and Transport of Correlated Electronic States at Room Temperature in Graphene Bilayers, (05 2010)
05/18/2010	5.00	M. Gilbert. Performance Characteristics of Scaled Bilayer Graphene Pseudospin Devices, (05 2010)
08/30/2011	6.00	John Shumway, Matthew Gilbert. Effects of Fermion Flavor on Exciton Condensation in Double Layer Systems, Physical Review Letters (08 2011)
08/30/2011	7.00	Brian Dellabetta, Matthew Gilbert. The Effect of Disorder on Superfluid Double Layer Graphene, Journal of Physics: Condensed Matter (08 2011)
08/30/2011	8.00	Youngseok Kim, Allan MacDonald, Matthew Gilbert. Pseudospin Torques in Semiconductor Bilayers, Physical Review B (08 2011)
11/06/2012	9.00	Youngseok Kim, Ewelina M. Hankiewicz, Matthew J. Gilbert. Topological Excitonic Superfluids in Three Dimensions, Physical Review B (04 2012)
11/06/2012	12.00	Zachary J. Estrada, Brian Dellabetta, Umberto Ravaioli, Matthew J. Gilbert. Phonon Limited Transport in Graphene Pseudospintronic Devices, IEEE Electron Device Letters (10 2012)
TOTAL:	**10**	

Number of Manuscripts:

Books

Received	Paper
TOTAL:	

Patents Submitted

Patents Awarded

Awards

Graduate Students

NAME	PERCENT_SUPPORTED	Discipline
Brian Dellabetta	0.50	
Youngseok Kim	1.00	
Zachary Estrada	1.00	
FTE Equivalent:	**2.50**	
Total Number:	**3**	

Names of Post Doctorates

NAME	PERCENT_SUPPORTED
Hsiang-Hsuan Hung	0.50
FTE Equivalent:	**0.50**
Total Number:	**1**

Names of Faculty Supported

NAME	PERCENT_SUPPORTED
FTE Equivalent:	
Total Number:	

Names of Under Graduate students supported

NAME	PERCENT_SUPPORTED
FTE Equivalent:	
Total Number:	

Student Metrics

This section only applies to graduating undergraduates supported by this agreement in this reporting period

The number of undergraduates funded by this agreement who graduated during this period:	0.00
The number of undergraduates funded by this agreement who graduated during this period with a degree in science, mathematics, engineering, or technology fields:.....	0.00
The number of undergraduates funded by your agreement who graduated during this period and will continue to pursue a graduate or Ph.D. degree in science, mathematics, engineering, or technology fields:.....	0.00
Number of graduating undergraduates who achieved a 3.5 GPA to 4.0 (4.0 max scale):	0.00
Number of graduating undergraduates funded by a DoD funded Center of Excellence grant for Education, Research and Engineering:	0.00
The number of undergraduates funded by your agreement who graduated during this period and intend to work for the Department of Defense	0.00
The number of undergraduates funded by your agreement who graduated during this period and will receive scholarships or fellowships for further studies in science, mathematics, engineering or technology fields:	0.00

Names of Personnel receiving masters degrees

NAME
Zachary Estrada
Total Number: 1

Names of personnel receiving PHDs

NAME
Total Number:

Names of other research staff

NAME	PERCENT_SUPPORTED
FTE Equivalent:	
Total Number:	

Sub Contractors (DD882)

Inventions (DD882)

Scientific Progress

See attachment

Technology Transfer

I. FINAL PROGRESS REPORT FOR GRANT NUMBER W911NF-09-1-0347

The aim of this project is to explore the strongly correlated states, more specifically Bose-Einstein condensation of indirectly bound excitons, in bilayer graphene. During this final reporting period, we have continued our work on the extention of the many-body calculations to an atomistic model, examined the electron-phonon coupling, studied the possibility of finding the same type of condensation in a 3D topological insulator, and started our work on a time-dependent theory to understand the behavior of the time-dependent many-body systems. In this final progress report, we will outline our most important results and draw some final conclusions from our 3 year project.

II. OVERALL SCIENTIFIC ACCOMPLISHMENTS

A. Overall Scientific Accomplishments: Electron-Phonon Interactions in Dipolar Superfluids

In Fig. 1, we show a schematic of the graphene pseudospin (G-PsS) device we consider to understand the role of the electron-phonon interaction in multi-layer graphene structures. The proposed device is comprised of two monolayers of graphene with lengths of 30 nm and widths of 10 nm. The layers are considered to be perfectly registered ideal sheets of zigzag graphene, such that the lattice sites of each layer are aligned. Each monolayer is terminated with an independent set of metal contacts from which current may be injected and extracted. We assume an ideal model for these contacts, which do not cause unintentional doping of the graphene layers[1]. The graphene monolayers are separated by a 1 nm layer of SiO_2 which serves as a tunnel dielectric with a corresponding single particle tunneling amplitude of Δ_{sas} = 1 μeV. Each layer is individually gated to independently control the layer carrier concentrations with the gates separated from the layers by 20 nm of SiO_2. In order to most effectively drive the interlayer condensate current, we apply the bias voltage in the drag-counterflow configuration[2] in which positive interlayer voltage is applied to the top left contact (V_{TL}) and an equal negative interlayer bias is applied to the top right contact (V_{TR}) while the contacts in the bottom layer remain grounded ($V_{BL} = V_{BR} = 0\ V$). The interlayer current discussed here is then measured flowing from the top left contact to the bottom left contact.

To model our system, we use a tight-binding Hamiltonian to represent each of the layers

$$H_{layer} = \sum_{<i,j>} \tau \mid i\rangle\langle j \mid + V_i \mid i\rangle\langle i \mid, \tag{1}$$

where lattice points i and j are first nearest neighbors. $\tau = -3.03eV$ is the nearest neighbor hopping energy for the p_z orbital of graphene, which allows for the unique low-energy linear dispersion at the K and K' points in the

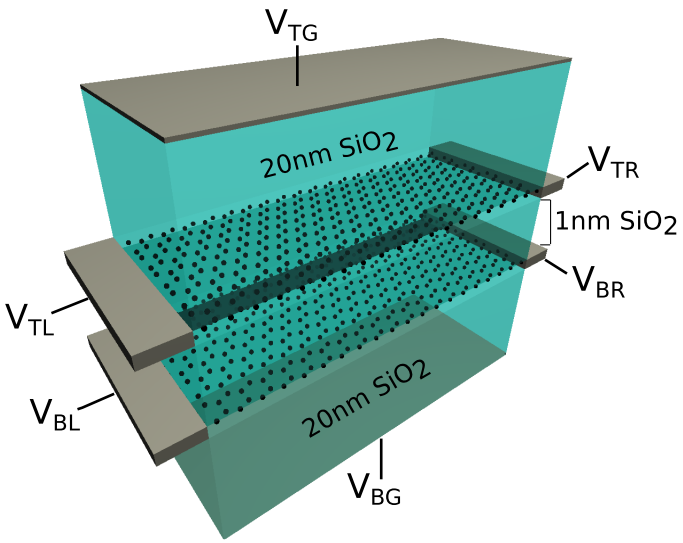

FIG. 1. Schematic illustration of the device under consideration in this work. Here we have two monolayers of graphene separated by 1 nm SiO_2. Each layer has a separate set of contacts (V_{TL} and V_{TR} for the top layer and V_{BL} and V_{BR} for the bottom layer) from which current may be injected and extracted. Top and bottom gates, V_{TG} and V_{BG}, are used to adjust the layer carrier concentrations.

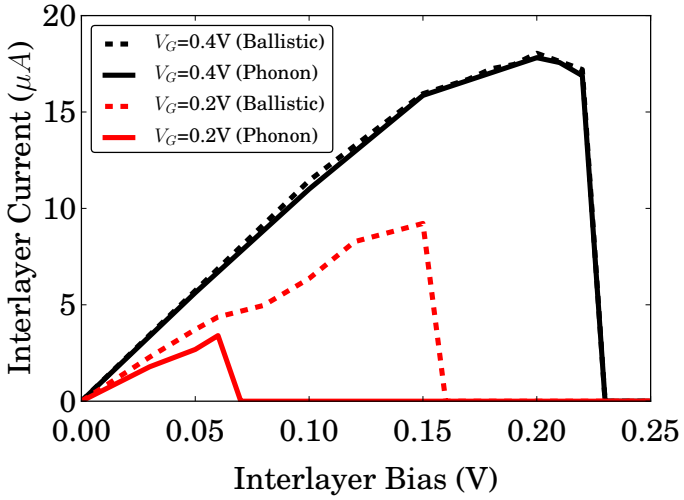

FIG. 2. Current-Voltage characteristic obtained from NEGF simulations comparing ballistic (dotted lines) and phonon cases (solid lines) for two gate voltages, V_G=0.4V (black) and V_G=0.2V (red).

Brillouin zone. The full system Hamiltonian is formed as

$$\mathcal{H}_{sys} = \begin{bmatrix} H_{layer} & 0 \\ 0 & H_{layer} \end{bmatrix} + \sum_{\mu=x,y,z} \hat{\mu} \cdot \mathbf{\Delta} \otimes \sigma_\mu, \tag{2}$$

with the interlayer interactions including both single particle tunneling and the mean-field many-body contribution, $\mathbf{\Delta}$, coupling the two layers using a local density approximation, which drives the phase transition[?]. In Eq. (2), μ represents a vector that isolates each of the Cartesian components of the pairing vector, and σ_μ represents the Pauli spin matrices in each of the three spatial directions. The on-site potential energy V_i is calculated via a 3-dimensional Poisson solver. The transport quantities are calculated via the non-equilibrium Green's function (NEGF) formalism[3] self-consistently with the interlayer interactions and the electrostatics. We introduce carrier-phonon scattering to our Hamiltonian within the self-consistent Born approximation. We include the relevant self-energy terms for both elastic acoustic phonon scattering (with deformation potential $D_{ac} = 19$ eV)[4] and inelastic optical phonon scattering processes (with optical deformation potential $D_{op} = 1\text{x}10^9$ eV/cm and energy $\hbar\omega_0 = 164.6$ meV)[5], in which both interband and intraband scattering are included by utilizing a real-space basis[6]. We have set the system temperature to be T_{sys} = 300 K for all calculations.

In G-PsS devices, the most important parameter to device performance is the critical current (I_c), or the maximum interlayer current that the system can sustain by adjusting the interlayer phase relationship. I_c is defined as[?]

$$I_c \sim \frac{qW\rho_s}{\hbar L_c}. \tag{3}$$

In Eq. (3), q is electronic charge, W is the width of the system, ρ_s is the pseudospin phase stiffness, and L_c is the coherence length. The coherence length in pseudospin systems expected to form a condensate phase, defines the maximum length which quasiparticles propagate in the system before undergoing retroreflection. When a quasi-particle is retroreflected, the system launches an exciton to conserve current[?]. The process is similar to Andreev reflections in a superconductor, except that here electrons are injected in one layer and are reflected as electrons with opposite momentum in the other layer. The coherence length is inversely proportional to the Fermi wavenumber (k_F) and is approximately given by[?]

$$L_c \sim \frac{1}{k_F}\sqrt{\frac{\rho_s}{\Delta_{sas}}}. \tag{4}$$

The critical current is defined as the maximum interlayer current attained before self-consistency is lost. After the system passes the interlayer voltage corresponding to the critical current, the interlayer current drops sharply as the system can no longer sustain the condensate phase and interlayer tunneling becomes dominated by single particle tunneling[? ?]. We plot the interlayer current-voltage characteristic calculated for two values of gate voltage in Fig. 2. We first examine the critical current with a gate voltage of $V_{TG} = -V_{BG}$ (hereafter referred to as V_G) = 0.40 V, a value

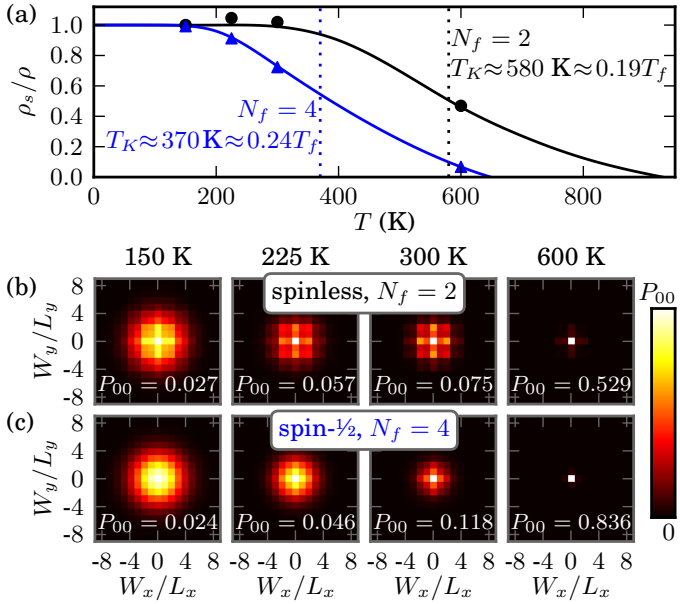

FIG. 3. (color online) (a) Superfluid fraction for spinless (black circles, $N_f = 2$) and spin-$\frac{1}{2}$ (blue triangles, $N_f = 4$) symmetric double-layer electron-hole condensate, calculated from PIMC simulations of 40 electron-hole pairs. Estimates of T_{KT} are made where the superfluid fraction drops to $1/2$, and lines are a guide to the eye. Normalized historgrams of topological winding distributions, which measure superfluid density, Eq. (5), for the (b) spinless and (c) spin-$\frac{1}{2}$ case.

chosen to place the system well within the predicted regime for room-temperature superfluidity[7] . We find that the critical current for the ballistic case is $I_c \approx 18.4\mu A$, in good agreement with the analytic value of $I_c^A \approx 19.5\mu A$ while $I_c^{ph} \approx 17.9\mu A$ when the phonon interactions are included representing a change of only 2.7%. At V_G = 0.20 V, we find a critical current of $I_c \approx 10.0\mu A$ for the ballistic case and $I_c^{ph} \approx 3.4\ \mu A$ when phonon interactions are included, a 66.0% drop in critical current. This work demonstrates that if the graphene bilayer is operated at high gate voltages, then the effects of phonon scattering can be minimized.

B. Overall Scientific Accomplishments: Phase Transitions with Increased Fermion Flavor

Interest in dipolar superfluids has received increased due in large part to the prediction of dipolar superfluid behavior at or above room temperature in double layer graphene[7–9]. This is uniquely possible in graphene due to the symmetric linear band-structure and ability to sustain large carrier concentrations in two closely-spaced layers. Yet, this prediction is not without significant controversy. As superfluidity is predicted to occur in the double layer graphene system outside of the quantum Hall regime, additional fermion flavors—beyond the top or bottom layer freedom—may participate in the phase transition. Theoretical disagreements over the Kosterlitz-Thouless transition temperature (T_{KT}) arise from differing assumptions about the importance of these extra flavors for screening in dipolar exciton condensates. In the works predicting a high transition temperature of $T_{KT} \approx 0.1\ T_F$ (where T_F is the system Fermi temperature) the fermionic degrees of freedom in the system were taken to be strongly correlated in a gapped condensate phase and could not screen enough to significantly lower T_{KT}. Other works that predict a low transition temperature of $T_{KT} \approx 10^{-7}\ T_F$ assume that screening from additional degrees of freedom add independenty to effectively screen out the the interlayer interaction[10,11]. While experiment will be the ultimate arbiter of the value of T_{KT}, many-body theoretical approaches will play a significant role in understanding the nature of the of the phase transition.

In Fig. 3 (a), we show our calculated superfluid fraction as a function of the system temperature. Our calculations reveal a suppressed T_{KT} when the additional spin degree of freedom is included. Superfluid fraction is an excellent way to understand phase transitions in systems as it saturates at 1 for low temperatures and asymptotes to 0 beyond the phase boundary. We denote the T_{KT} as the temperature where the superfluid fraction has dropped to 0.5 to be consistent with previous work[12]. We see a clear drop in T_{KT} from $T_{KT} \approx 580$ K in the spinless case to $T_{KT} \approx 300$ K in the spin-$\frac{1}{2}$ case, illustrating the effect of increased fermion flavor on the phase transition. In fact, this drop in transition temperature may be understood without resorting to screening arguments. One would expect a decrease in T_{KT} simply from reduced quantum degeneracy as more fermion flavors are added. In an ideal Bose gas, the

magnitude of the transition temperature is determined by the condition $n\lambda(T_{KT})^2 \sim 1$, where $\lambda(T) \sim T^{-1/2}$ is the thermal deBroglie wavelength and n is the density of identical Bosons. As fermions pair into bosons, there must be at least N_f distinguishable species of bosons, decrease the density n and hence, the transition temperature T_{KT} by $1/N_f$. This effect of reduced quantum degeneracy degeneracy can also be seen by comparing T_{KT} to the Fermi temperature (at our density, $T_F^{ns} = 3086$ K and $T_F^{sp} = 1543$ K); in each case our estimated T_{KT} is around four or five times smaller than T_F.

The calculated superfluid fraction is estimated by the presence of permuting paths that wind around the periodic box[13]. In two dimensions, the superfluid fraction is given by,

$$\frac{\rho_s}{\rho} = \frac{mk_BT}{\hbar^2(N_e + N_h)} \langle W_x^2 + W_y^2 \rangle. \tag{5}$$

In Eq. (5), W_x and W_y are the topological windings (which are integer multiples of the supercell dimensions) corresponding to the different path configurations. Note that for excitonic condensates, we use the number-coupled winding, where W_x and W_y each include a sum over individual windings of electron and hole quasi-particles.

In Fig. 5, the bottom two rows, (a) and (b) compare the exciton winding probabilities for the spinless (a) and spin-$\frac{1}{2}$ (b) for several temperatures. At $T = 150$ K, we see similar behavior for both systems, as each system is nearly all superfluid. Careful examination shows the histogram for the spinless case have extra even-odd structure. In an exciton, electrons pair with the holes and wind as a composite particle giving rise to peaks in the winding histogram at even integers. Thus showing clear evidence the system is an exciton condensate. The even-odd effect is more washed out in the spin-$\frac{1}{2}$ state, which we attribute to the relatively small number, ten, of identical fermions. Larger simulations should sharpen this even-odd signature of an excitonic condensate. Note that biexcitons would have strong peaks at multiples of four; we do not see evidence of a biexcitonic condensate in our simulations.

Next we examine real-space static correlation among the quasiparticles, due to Coulomb interactions and Pauli exclusion. We have collected the pair-correlation functions $g(r)$, which are easily calculated in PIMC by binning the equal-time pair distributions in a histogram. In contrast to other QMC methods, such as variational or diffusion Monte Carlo, there is no bias from a trail wavefunction, thus PIMC gives essentially exact pair correlations, aside from errors associated with the fixed-node approximation. In Fig. 4 we show our calculated pair correlation functions at $T = 150$ K. We find the presence of an exchange hole in between identical fermions, which is larger in the $N_f = 4$ case simply because the density of particles of a particular flavor decreases as $1/N_f$. We find that there is a strong, attractive, interlayer correlation g^{eh}, with a peak at small separations that is coincident with the formation of indirectly bounds excitons with holes in the top layer sitting directly above the electrons in the bottom layer. This pairing of identical spin states in the $N_f = 4$ case may be an artifact of our nodal model, where we have built or nodal wavefunction from a Slater determinant of orbitals pairing like spins only.

Interestingly, we find a small correlation hole for the $N_f = 4$ case, arising almost equally from the electron and hole of opposite spin: the particle in the same layer (with the same charge) is slightly repelled, while the particle in the opposite layer (with the opposite charge) is similarly attracted. This is a clear demonstration extra fermion flavors correlate among each other, even when they do not bind as condensed excitons. This is more dramatically illustrated in Fig. 4 (c) and (d). In Fig. 4, we plot the intralayer pair correlation in 2D corresponding to $g_{sp}^{\uparrow\uparrow}$ and, as expected, we see a large correlation hole where Pauli exclusion and Coulomb repulsion forces other identical particles apart. However, when we include spin-$\frac{1}{2}$ particles and examine the intralayer correlation of $g_{sp}^{\uparrow\downarrow}$ in Fig. 4 (c), we see a much weaker correlation hole. Note that we again do not see evidence of biexciton formation, which would appear as a positive correlation of like-charged, opposite-spin particles in the same layer[?] .

We do not see a large drop in T_{KT} as predicted in Refs. 10 and 11. In an effort to understand this, we explore the dynamic correlation functions, namely the polarizability. In Refs. 10 and 11, the large-N_f approximation strongly resembles the random phase approximation (RPA), and hence the screening they find is essentially the Lindhard function, with suppression of screening at very small q due a BCS-like excitonic condensate. In Fig. 5, we show that our calculated polarizabilities are considerably different. To collect the dynamic correlation functions we sample the polarization operator between different fermion flavors γ and γ',

$$\Pi_{\gamma\gamma'}(\mathbf{q}, i\omega_n) = -\frac{q_\gamma q_{\gamma'}}{V\hbar} \int_0^{\beta\hbar} \langle T_\tau \; n_{\mathbf{q},\gamma}(\tau) n_{-\mathbf{q},\gamma'}(0) \rangle \; d\tau, \tag{6}$$

where $n_{\mathbf{q},\gamma} = \sum_{i=1}^{N_\gamma} e^{i\mathbf{q}\cdot\hat{\mathbf{r}}_i}$ is the density operator for fermion flavor γ.

In Fig. 5 we show the $\Pi_{\gamma,\gamma'}(\mathbf{q}, 0)$ between different fermion flavors normalized by the 2D density of states as a function of wavelength normalized by the Fermi wave vector at a system temperature of $T = 150$ K. Here we find the polarization response from identical particles in $N_f = 2$ and $N_f = 4$ track the Lindhard function very well in the short wavelength limit, past $q > 2k_f$, as one would expect from Fermi liquid theory.

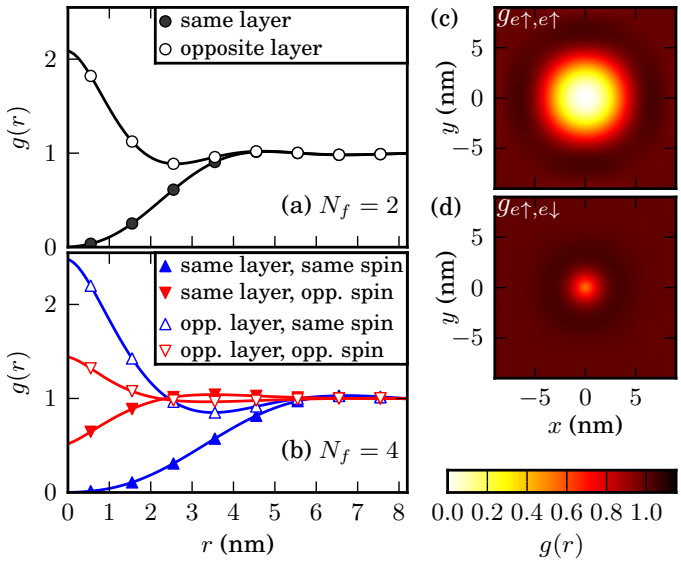

FIG. 4. (color online) Radial pair correlation functions for (a) spinless, $N_f = 2$, and (b) spin-$\frac{1}{2}$, $N_f = 4$ cases. (a) Intralayer exchange-correlation hole for the same spin species, $g^{\uparrow\uparrow}(\mathbf{r}_{ij})$. (d) Intralayer correlation hole for opposite spin species, $g^{\uparrow\downarrow}(\mathbf{r}_{ij})$.

Interestingly, we find similar behavior for both $N_f = 2$ and $N_f = 4$ in response to long wavelength excitations ($q \to 0$). This is expected as we are clearly in the condensate regime in which all carriers should be paired into excitons and, therefore, unable to respond to perturbations. The response between particles in different layers or of different spin is negative, indicating that these correlations suppress screening from the independent particle, RPA response. The response of the exciton is quite strong, which the opposite-spin flavors have a weak negative response, Fig. 5(b). We have calculated the polarizabilities at temperatures both above and below T_{KT}, and found very little difference between the different temperature traces for both the $N_f = 2$ and $N_f = 4$ cases, indicating that the screening behavior is dominated by pre-formed excitons, with exist above T_{KT}.

However, Fig. 5(c) shows that the sum of inter- and intra-layer polarizabilities for $N_f = 4$ is smaller than that of $N_f = 2$. While the large-N calculation finds enhanced screening with more fermion flavors N_f which grows as N, but we find a weaker trend. The reason for this difference is excitonic binding and correlation between different. In the large-N expansion, the starting point is RPA like screening. Because each flavor can screen independently, it has been argue that the Coulomb interaction because too weak to form pairs, except for weak BCS pairing of states near the Fermi surface when the temperature is below T_{KT}. In our simulations, our model has strong excitonic pairing. The pairing of charge into neutral excitons suppresses their ability to screen. This excitonic pairing and correlation between quasiparticles of different spin is not present in the large-N_f approximation's perturbative expansion.

This work shows that the phase transition in very closely separated layers of graphene is not possible at room temperature. This is because the exciton condensate is not an effective screener of additional fermion flavors present in the graphene system. That said, the most interesting scientific breakthrough this year has been the successful implementation of linear response theory within PIMC. It has given us a tool to examine very interesting and experimentally relevant phenomena without needing a large number of approximations and with full many-body interactions.

C. Overall Scientific Accomplishments: Transport in Clean and Disordered Zero-Field Semiconductor Bilayer Systems

For almost two decades coupled semiconductor quantum well systems have revealed interesting effects deep within the quantum Hall regime. Comparatively speaking, there have been relatively few studies of the bilayer system outside of the quantum Hall regime. Here we do not expect to see a phase transition, but the system may still exhibit transport properties similar to those characteristic of the quantum Hall pseudospin ferromagnets, such as an enhancement on interlayer tunneling conductance[14]. Previous mean-field calculations show that semiconductor bilayers may exhibit interlayer exchange enhancement characterized by enhancement factor S, but the value of S is moderate[15]. Following their work, we examine the interlayer transport properties of both clean and disordered semiconductor bilayer systems without magnetic fields. We find that transport characteristics similar to quantum Hall ferromagnets may persist outside of the quantum Hall regime and we discuss how the the physical properties

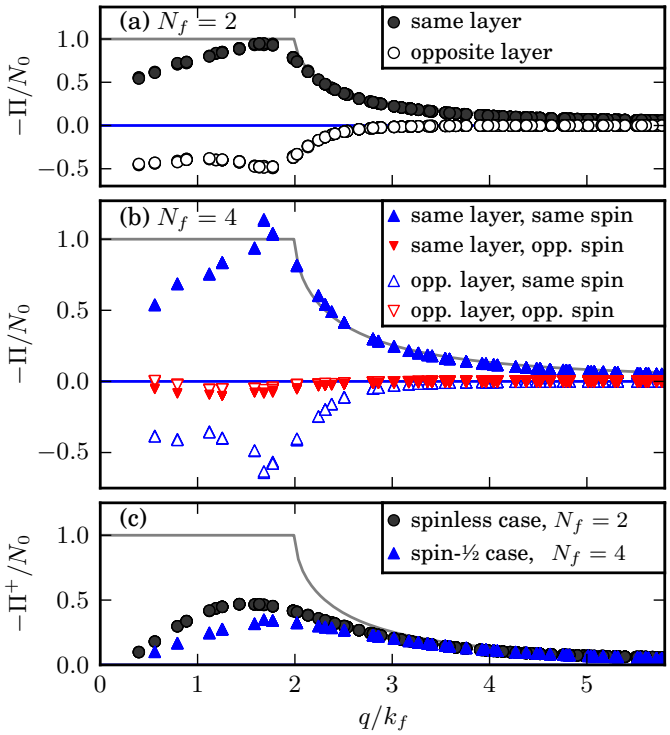

FIG. 5. (a) Interlayer and intralayer polarizabilities for $N_f = 2$ versus the perturbation wavevector normalized by the Fermi wave vector. (b) Interlayer and intralayer polarizabilities for $N_f = 4$ normalized by the Fermi wave vector. (c) Sum of the interlayer and intralayer polarizabilites for $N_f = 2$ and $N_f = 4$ normalized by the Fermi wave vector. In each plot the polarizabilities are plotted against the Lindhard response function (grey line) in 2D and have been normalized by the density of states at the Fermi energy in 2D, N_0.

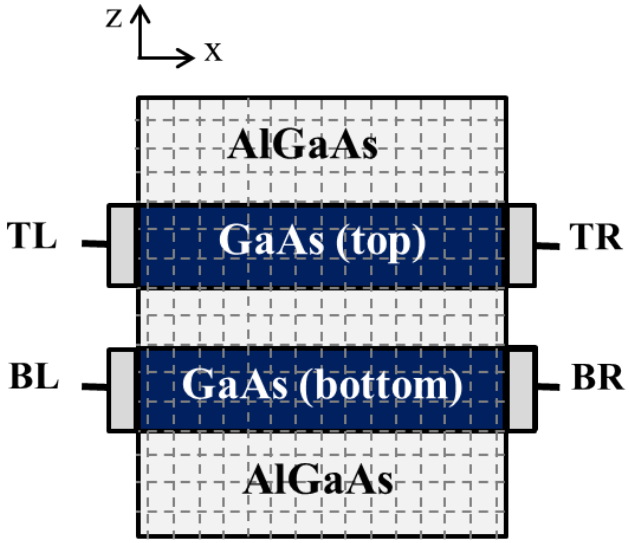

FIG. 6. Device cross-section in x, z direction. Top and bottom $Al_{0.9}Ga_{0.1}As$ barrier thickness is 60 nm, GaAs quantum well thickness is 15 nm, and $Al_{0.9}Ga_{0.1}As$ barrier thickness is 1 nm. A channel is 1.2 μm long and 7.5 μm wide. An assumed electron density in 2 dimensional electron gas (2DEG) is $2.0 \times 10^{10} cm^{-2}$.

of these exchange enhanced transport signatures change as we include material disorder. This work is of particular importance as it provides us with a system which is both experimentally realizable and readily accessible to experimentalists. We study this system to provide a pathway to understand the validity of our graphene theory in the

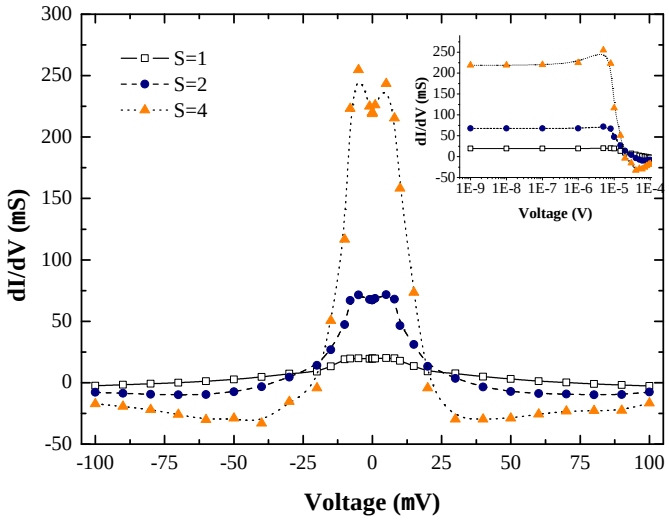

FIG. 7. Plot of the differential conductance of the bilayer system at $S = 4$ (orange triangle), $S = 2$ (blue circle), and $S = 1$ (opened rectangular) as a function of interlayer bias $V_B - V_T$ at 0K. In the inset, the same plot in negative interlayer bias with same y axis is plotted with x axis in log scale. In small bias window, almost constant interlayer transconductance is observed. After the interlayer bias reaches $V_{INT} \approx 10\mu V$, an abrupt drop in transconductance can be seen in the interacting electron cases of $S = 2, 4$. We plot the differential conductance on a logarithmic scale in the inset figure to clearly illustrate the observed drop in interlayer conductivity.

absence of graphene experiments and with the effects of screening making the observation of the condensate phase doubtful.

A schematic feature of our device is presented in Fig. 6. In this work, we consider for an $Al_{0.9}Ga_{0.1}As/GaAs$ bilayer heterostructure with 60 nm top and bottom $Al_{0.9}Ga_{0.1}As$ barriers which act to isolated the coupled quantum wells from electrostatic gates. Our system is comprised of two 15nm deep GaAs quantum wells with a 1 nm $Al_{0.9}Ga_{0.1}As$ barrier between the two quantum wells. Since bilayer experiments have taken place at very low temperature around a few tens of mK, we may write the Hamiltonian in the form of decoupled 1D longitudinal channels in transport ($\hat{x}$) direction taking account of eigenenergy of transverse ($\hat{y}$) direction properly[16]. The system is coupled with a 3D Poisson solver to correctly account for the electrostatics. Bottom contacts are biased and current is extracted out from top contacts ($V_{BL} = V_{BR} = V_{INT},\ V_{TL} = V_{TR} = 0$). From our analysis, the critical current of this system is determined by single particle tunneling amplitude and enhancement factor S. The resulting critical currents are $I_c = 1.80,\ 4.52\ nA$ for $S = 2,\ 4$ respectively which show a good agreement with mean-field calculation results, $I_c^A = 2.14,\ 4.00\ nA$.

To get a clear picture of how interlayer interactions modify the resultant interlayer transfer characteristics, we force the system out of the linear response regime. In Fig. (7) , we compare the interlayer transport result with the non-interacting case ($S = 1$). We see that all of the curves are sharply peaked near zero bias, more strongly in the case of the interacting-system simulations ($S = 2, 4$) which is expected. After the critical current, we see that the interlayer conductivity drops appreciably, as is the case in graphene or the quantum Hall system. However, the important thing to point out here is that the semiconductor bilayer system has a critical current which does not occur when the in-plane pseudospin phase angle reaches $\frac{\pi}{2}$. This is due to the charge imbalance which develops between the layers causing the out-of-plane pseudospin field to precess faster separating the layers energetically with smaller applied interlayer bias.

With our understanding of the system in clean limit, we are interested in AlGaAs/GaAs system with impurities which is naturally occurred during a fabrication. In order to simulate device characteristics, we adopt a model of ionized impurities and roughness at the interface of heterojunction in AlGaAs/GaAs system[17]. Random disorders can be inserted into the system Hamiltonian by adding uniform distribution having a window defined by mean free path, Λ. The simulation is carried out with NEGF formalism in two dimensions coupled with 3D Poisson solver. A mean free path we examine in this study adds a significant amount of perturbation into onsite energy up to $\sim 20\%$ of the self-consistent Hartree potential at clean limit. The perturbation in turn affects the expectation values of the in-plane and out of plane pseudospin fields and alters transport characteristics of the system. Clearly, disorder causes some localization in the transport ($\hat{x}$) directional pseudospin fields and pseudospin angles of transport orbital are no longer well aligned and locally precessed even at the low bias window. The overall effect of disorder results in enhancement on interlayer tunneling, but less than the enhancement in clean limit. The random scatterers are added

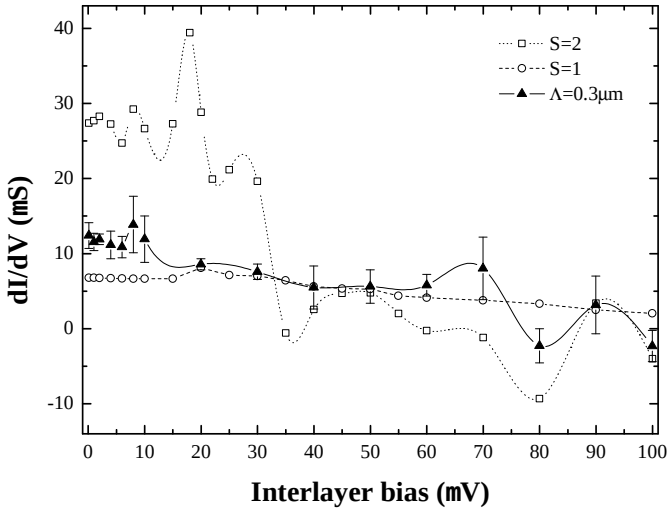

FIG. 8. Plot of differential conductance as a function of interlayer bias. We plot clean limit of assumed enhancement factor $S = 2$ with non-interaction case $S = 1$. We also present a result with a disorder level of $\Lambda = 0.3\ \mu m$ with error bars from four different disorder configurations. Simulation conditions: Interlayer bias is only applied at $V_{BR} = V_{INT}$, and rest of the contacts is zero. An assumed 2DEG density is $n_e = 3.0 \times 10^{-10} cm^{-2}$ and quantum well has $Length = Width = 1.2\ \mu m$.

up to $\Lambda = 0.3\ \mu m$ and the end result is a reduction of the interlayer conductance to its non-interacting value as shown in figure 8. The second major effect of the disorder is broadening of tunneling peak described by $\Gamma = \hbar/\tau$ where τ is quantum life time[18]. The predicted broadening ($\Gamma/2$) for $\Lambda = 0.3\ \mu m$ is around $82\ \mu eV$ and corresponding result from NEGF calculation lies roughly around $80\ \mu eV$ in Fig. 8. This indicates that the interlayer transport is no longer controlled by single particle tunneling amplitude and instead is controlled by the material disorder.

This work gives an insight into electron-electron bilayer system under zero-magnetic field, a system which is experimentally realizable.. We find that interlayer transport in this system is limited by the strength of correlation between two layers and charge imbalance of the system. We find localized pseudospin field with disorder and their net effect suppresses coherent tunneling transport. With significant amount of disorder, interlayer transport tends to be dependent on material disorder.

D. Final Scientific Accomplishments: Dipolar Superfluids in Disordered Systems

Our simulations in the ideal system show two different regions in the graphene bilayer - a region near the contacts where injected carriers trigger a crossed Andreev Reflection event and the channel region where all transport is attributed to superfluid current. When an electron is injected with energy lower than the superfluid gap, it will trigger an Andreev Reflection similar to what happens in a superconductor. In the exciton superfluid case, however, an injected electron will drive an exciton across the channel, with a retroreflected hole coming out the bottom left contact to conserve momentum. The effect of the crossed Andreev reflection is thus a superfluid intralayer current and the quasiparticle interlayer current. The quasiparticle current evanescently decays into the channel, penetrating a certain length into the superfluid region. This distance, known as the coherence length, is found to be $L_c = 5\ nm$. We use this observation to break down the disordered case study into two scenarios - where disorder is located only in the coherence length (Contact Disorder) and where disorder is located away from the coherence length (Channel Disorder).

The main results of our work are shown in Fig. 9. At a vacancy concentration of 0%, the critical current is $18.4\ \mu A$. To the left of the ideal point we plot the effect of channel disorder on critical tunneling current. We find that vacancies induce a local density of states (LDOS) in graphene layers that bring about occupied states within the superfluid gap and act to locally lower the superfluid density, m_{exc}. For small vacancy concentrations (1% vacancies placed randomly throughout the channel), this has little effect on m_{exc} because the disorder is sufficiently isolated. However, as the channel is made more disordered, superfluid density begins to drop non linearly in the channel. The average superfluid density saturates, however, due to the unchanging contribution from the ideal contact regions, decreasing to roughly 70% of its value at a 4% vacancy concentration. Because critical tunneling current is proportional to m_{exc}, we find good agreement with this explanation via the approximate square-root dependence seen in Fig. 9. The error bars show that the configuration of the disorder has little effect on I_c, as average superfluid density remains robust

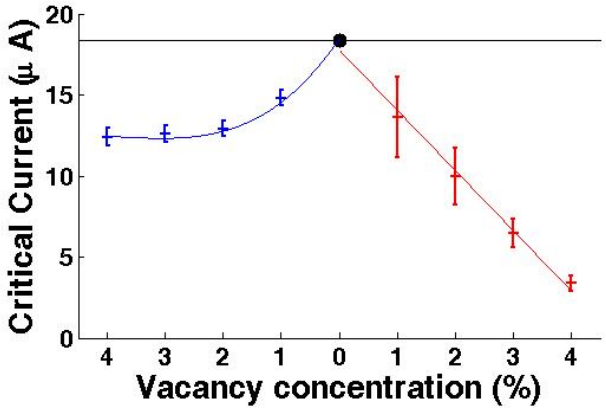

FIG. 9. Statistical variation of critical interlayer current for several runs at the bias just before the condensate is broken. Vacancies which are more than a distance of one coherence length away from the top layer contacts are to the left of the ideal (0%) case, depicted by a black circle, while vacancies which are within one coherence length from the top layer contacts are to the right. The excitonic condensate is lost in both cases for top layer vacancy concentrations larger than 4%. The solid lines represent analytic calculations for I_c with modified values of superfluid density (blue line) and width (red line).

regardless of the disorder's random configuration. In both cases, no self-consistent solution was found for vacancy concentrations greater than 4%.

We see a clear linear dependence in the contact disordered regime. Injected carriers become increasingly likely to be backscattered by the impurities near the contacts before Andreev reflection can occur. This results in a significant reduction in the area in which quasiparticle tunneling can occur near the contact, reducing interlayer conductivity significantly. As critical tunneling current is linearly dependent on the width of the system, this provides a simple explanation for the physics of the linear decrease in I_c. Assuming that each vacancy removes 0.5 nm of effective width from the system, we plot the resulting relationship in Fig. 9 with a red line denoting I_c^A with a decreasing width. Deviation in I_c, as seen by the large error bars in the contact disordered case, is attributed to the non linear randomized bunching of disorder.

This work[19] provides a comprehensive study on the effect of short-range scatterers in double layer graphene systems that must be taken into account for this system to be experimentally realized. Unfortunately, room temperature condensation is subject not only to defects in fabrication, but also carrier-phonon interactions.

E. Overall Scientific Accomplishments: Dipolar Superfluids in 3D Time-Reversal Invariant Topological Insulators

Spatially segregated monolayers of graphene have been both theoretically[7–9] and experimentally[20] explored for signatures of excitonic superfluidity. While signs of interlayer correlation are experimentally observed, additional fermionic degrees of freedom, or flavors, screen the strength of the interlayer interaction[21] making the observation of dipolar exciton superfluid in graphene multilayers challenging.

The advent of time-reversal invariant topological insulators (TI)[22,23] has brought renewed interest in finding DES in condensed matter systems. In sufficiently thin TI films, it has been proposed that spatially segregated surface electrons and holes may bind into a topological dipolar intersurface exciton superfluid (TDIES). To this point, existing approaches to TDIES have considered strictly two-dimensional Dirac surface states separated by an insulating spacer[24–28]. Yet the existence of a TDIES in three-dimensions is not a foregone conclusion based on two-dimensional surface state analysis. The most obvious drawback being that in a 3D TI, each of the surfaces is interconnected and there exists no obvious mechanism to segregate the electron and hole layers, as in other proposed systems.

We begin in Fig. 10, where we schematically show the system we consider. We apply top and bottom potentials of opposite polarity to induce electrons on the top surface and holes on the bottom surface. We attach contacts C1 - C4 to the top and bottom surfaces on the left and right sides of the TI through which current may be injected and extracted as seen in Fig. 10. As for the major findings resulting from this work, we find that the proper exciton pairing order parameter is purely imaginary which is necessary to properly account for the system dynamics. Furthermore, we find that the exciton order parameter is p-wave and that electrons will only bind with holes of the same chirality from different orbitals. We find that TDIES in time-reversal invariant TI thin films prefer to bind into excitons with a dominant many-body energy which prevents single particle intersurface transport as the intersurface polarizablity drops to zero. This allows for the observation of superfluid behavior out of the quantum Hall regime and without

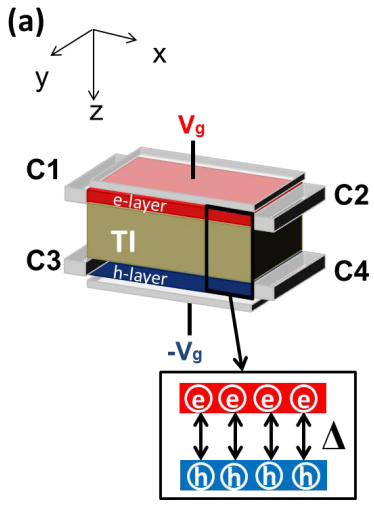

FIG. 10. Schematic of topological insulator thin-film system under consideration. The top and bottom surfaces are assumed to contain equal numbers of electron and holes, respectively.

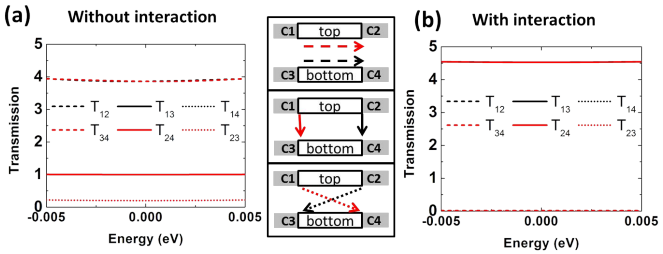

FIG. 11. A transmission between C1, C2, C3, and C4 of the system (a) without and (b) with intersurface interaction at a bias of $V_{bias} = 5\ mV$. (a): When there is no interaction and the system is not gapped, current flows across the device resulting in T_{12} (or T_{34}) dominating the transport. (b): When the system is gapped, however, the quasiparticle undergoes a similar process to Andreev reflections, resulting in large T_{13} and T_{24} as current flows from top surface to bottom surface with no transmission across either of the top T_{12} or bottom surfaces T_{34}.

the need to artificially segregate the surfaces. Finally, we find that the presence of a topological superfluid may be electrically detected by the presence of equal and opposite intersurface contact currents, as can best be seen from the individual transmission in Fig. 11.

III. FINAL CONCLUSIONS AND FUTURE OUTLOOK

The goals of this 3 year project have been to (i) analyze the physics of high-temperature superfluidity in bilayer graphene systems with a goal of understanding its role in post-CMOS architecture and (ii) develop the path integral quantum Monte Carlo technique as a new flexible approach for many-body quantum systems at finite temperature. With regards to the first goal of determining the role of segregated layers of tightly spaced graphene for post-CMOS architectures, the conclusions of our work show that the bilayer graphene system has transport properties in the superfluid phase which outperform other proposed post-CMOS devices. Yet our path integral quantum Monte Carlo calculations show that the superfluid phase transition is occluded by additional fermionic degrees of freedom and this effectively lowers the transition temperature to well below room temperature. We have shown that topological insulators provide a much more promising system for high-temperature device operation and these systems should be further explored. As to the second goal of this project, the development of efficient path-integral quantum Monte Carlo algorithms for finite temperature many-body simulations, we have successfully pushed this technique farther than ever before. In the sections outlined above, we have shown the ability to collect static and dynamic response functions for fermionic many-body systems to elucidate the superfluid transition temperature. This represents a powerful new technique from which the full interacting conductivity may be extracted. I feel that the best way

forward with regards to the path-integrals would be to take a step back from applying them to emergent systems, whose responses are not known, and calibrate the technique against other well-known systems such as Luttinger liquids in quantum wires.

---

[1] J. Cayssol, B. Huard, and D. Goldhaber-Gordon, Phys. Rev. B **79**, 075428 (2009).
[2] J. Su and A. H. MacDonald, Nat. Phys. **4**, 799 (2008).
[3] S. Datta, *Quantum transport : atom to transistor* (Cambridge University Press, Cambridge UK ;;New York, 2005).
[4] E. H. Hwang and S. Das Sarma, Physical Review B **77**, 115449 (2008).
[5] K. M. Borysenko, J. T. Mullen, E. A. Barry, S. Paul, Y. G. Semenov, J. M. Zavada, M. B. Nardelli, and K. W. Kim, Phys. Rev. B **81**, 121412 (2010).
[6] Y. Yoon, D. E. Nikonov, and S. Salahuddin, Applied Physics Letters **98**, 203503 (2011).
[7] H. K. Min, R. Bistritzer, J. J. Su, and A. H. MacDonald, Phys. Rev. B **78**, 121401 (2008).
[8] M. J. Gilbert and J. Shumway, J. Comput. Electron. **8**, 51 (2009).
[9] C. H. Zhang and Y. N. Joglekar, Phys. Rev. B **77**, 233405 (2008).
[10] M. Y. Kharitonov and K. B. Efetov, Phys. Rev. B **78**, 241401R (2008).
[11] M. Y. Kharitonov and K. B. Efetov, Semicond. Sci. Technol. **25**, 034004 (2010).
[12] E. L. Pollock and D. M. Ceperley, Phys. Rev. B **36**, 8343 (1987).
[13] D. M. Ceperley, Rev. Mod. Phys. **67**, 279 (1995).
[14] I. B. Spielman, J. P. Eisenstein, L. N. Pfeiffer, and K. W. West, Phys. Rev. Lett. **84**, 5808 (2000).
[15] L. S-acutewierkowski and A. H. MacDonald, Phys. Rev. B **55**, R16017 (1997).
[16] R. Venugopal, Z. Ren, S. Datta, M. S. Lundstrom, and D. Jovanovic, Journal of Applied Physics **92**, 3730 (2002).
[17] T. Ando and H. Tamura, Phys. Rev. B **46**, 2332 (1992).
[18] N. Turner, J. T. Nicholls, E. H. Linfield, K. M. Brown, G. A. C. Jones, and D. A. Ritchie, Phys. Rev. B **54**, 10614 (1996).
[19] B. Dellabetta and M. J. Gilbert, Journal of Physics: Condensed Matter **23**, 345302 (2011).
[20] S. Kim, I. Jo, J. Nah, Z. Yao, S. K. Banerjee, and E. Tutuc, Phys. Rev. B **83**, 161401 (2011).
[21] J. Shumway and M. J. Gilbert, Phys. Rev. B **85**, 033103 (2012).
[22] M. Z. Hasan and C. L. Kane, Rev. Mod. Phys. **82**, 3045 (2010).
[23] X. L. Qi and S.-C. Zhang, Rev. Mod. Phys. **83**, 1057 (2011).
[24] B. Seradjeh, J. E. Moore, and M. Franz, Phys. Rev. Lett. **103**, 066402 (2009).
[25] G. Y. Cho and J. E. Moore, Phys. Rev. B **84**, 165101 (2011).
[26] D. Tilahun, B. Lee, E. M. Hankiewicz, and A. H. MacDonald, Phys. Rev. Lett. **107**, 246401 (2011).
[27] Z. Wang, N. Hao, Z.-G. Fu, and P. Zhang, ArXiv:1106.5838.
[28] E. G. Moon and C. Xu, EPL **97**, 66008 (2012).